Optical Sensing near the Quantum Limit with Enhanced Dynamic Range by Resolving the Spectra of Interfering Photons

Russell M. J. Brooks,[1] Luca Maggio,[2] Thomas Jaeken,[1] Joseph Ho,[1] Erik M. Gauger,[1] Vincenzo Tamma,[2] and Alessandro Fedrizzi[1,*]

[1]*Institute of Photonics and Quantum Sciences, School of Engineering and Physical Sciences, Heriot-Watt University, Edinburgh EH14 4AS, United Kingdom*

[2]*School of Mathematics and Physics, University of Portsmouth, Portsmouth PO1 3QL, United Kingdom*

(Received 9 October 2025; revised 16 December 2025; accepted 20 January 2026; published 9 February 2026)

Optical sensing schemes based on two-photon interference offer a powerful platform for precision metrology, but are usually limited by a trade-off between dynamic range and measurement precision. Here, we overcome this limitation by resolving the frequency of two photons impinging on a beam splitter and combining these measurements with a new estimation strategy. This increases the usable dynamic range by up to a factor of 20 compared with conventional frequency nonresolved schemes. We implement the method with independent photon pair sources and characterize its performance in the presence of finite-resolution frequency-resolved detectors, which approach the quantum limit in the lossless regime. Our approach enables scan-free, nanometer resolution depth sensing over millimeter scale distances, with potential applications in biological and nanomaterial imaging.

DOI: 10.1103/6xy6-c2yd

Introduction—Two-photon interference is a consequence of the quantum nature of the electromagnetic field, and is foundational to many quantum optics experiments, from photonic quantum computing and communication to metrology and sensing [1–12]. Indistinguishable photons impinging on a balanced beam splitter manifest the nonclassical tendency to exit through the same output port from the destructive interference of the two-photon probability amplitudes [1–3,13]. This phenomenon has been exploited for precision estimation of optical path delays and coherence measurements, typically achieving subpicosecond [14–17] and recently attosecond temporal precision [18–20]. In comparison, direct time-of-flight using single-photon detectors is limited by detector jitter on the order of tens of picoseconds [21,22]. However, methods that rely on measuring only the photon statistics at the output of a beam splitter are limited by the photons' temporal bandwidth, which constrains the operational range and prevents sensitive measurements once the delay exceeds the coherence time [18,23,24].

Conventional multiphoton interference experiments do not resolve the photonic inner modes, such as frequency or time, which ignores the useful quantum information encoded within the photons [9,25]. It was shown theoretically in Ref. [25] that resolving the photon frequency can restore interference even between nonidentical photons and was later experimentally demonstrated between temporally distinguishable photons [26]. Similarly, frequency-resolved two-photon interference reveals quantum beat notes in the interferogram [27–29], in contrast to the single fringe of the nonresolved interferogram [1], accessing the spectral correlations that can be harnessed for precision metrology.

Recently, metrological schemes that sample the photonic inner modes have been shown to achieve the ultimate quantum-limited sensitivity in estimating conjugate variables, including time-frequency shifts [8,30], transverse position-momentum displacements [31,32], and full-state polarization [33]. In optical delay estimation, ideal frequency-resolved sampling offers uniform sensitivity across the entire delay range, unlike the nonresolved method, which is parameter dependent and must be optimized to reach maximum sensitivity [18]. However, these theoretical works require infinite resolving capabilities to fully erase information in the conjugate space and restore quantum interference [34,35]. In the absence of such devices, experiments are limited by finite resolution. The interference visibility depends on the spectral resolution, which must satisfy $\delta\omega \ll 1/|\Delta t|$ to restore interference with temporal delay Δt [8]. This has been studied using nondegenerate spectrally entangled photons [36], and weak coherent states [37].

In this Letter, we report on the metrological advantage of frequency-resolved sampling for optical delay estimation with independent, spectrally uncorrelated single-photon

*Contact author: A.Fedrizzi@hw.ac.uk

Published by the American Physical Society under the terms of the Creative Commons Attribution 4.0 International license. Further distribution of this work must maintain attribution to the author(s) and the published article's title, journal citation, and DOI.

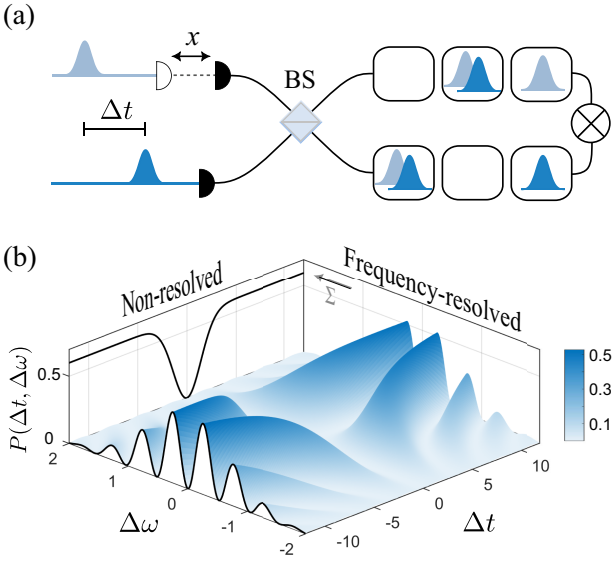


FIG. 1. (a) Two-photon interference setup. Two photons are input on a 50:50 beam splitter while a translation stage scans the path length delay x. The output ports are monitored by either bucket detectors or frequency-resolved detectors. (b) The two-photon frequency-resolved coincidence outcome probability, Eq. (2) is plotted as a function of the time delay Δt and frequency difference $\Delta\omega$, which exhibit fringes along planes of fixed time delay. Summing over all frequency differences (Σ) restores the nonresolved interferogram, which is projected onto the back panel.

states. We employ high-resolution ($6.9/2\pi$ GHz) frequency-resolved detectors, benchmark this method against a maximum-likelihood estimator without the spectral information, and realize more than a twentyfold increase in dynamic range and a thousand-fold improvement relative to other implementations [18–20]. We analyze the effects of finite frequency resolution on the Fisher information and discuss the practical utility of this technique for precision depth sensing.

Delay estimation—We now describe the method for estimating the relative time delay; full derivations are provided in Supplemental Material [38] (see also Ref. [39] therein). Consider two nonentangled photons arriving at separate ports of a balanced beam splitter at times t_1 and t_2, with a relative delay of $\Delta t = t_1 - t_2$, as shown in Fig. 1. Each photon has a Gaussian spectrum with a bandwidth given by the standard deviation σ and a corresponding temporal bandwidth $\tau = 1/2\sigma$. The distinguishability in all other degrees of freedom is characterized by the parameter $\eta \in [0, 1]$, with $\eta = 0$ representing complete orthogonality and $\eta = 1$ denoting perfect overlap. When the photons arrive simultaneously at the beam splitter, they interfere destructively and "*bunch*" into the same exit port with a probability determined by their temporal overlap. Temporal distinguishability leads to photons exiting different ports and subsequently being detected as a coincidence event. The photon-pair distribution after interference at the beam splitter is given by [18,24],

$$P_\delta^\eta(\Delta t) = \frac{1}{2}\left(1 + \delta\eta^2 e^{-\sigma^2\Delta t^2}\right), \tag{1}$$

where $\delta = +1, -1$ are the *bunching* or *coincidence* outcomes, respectively, of a single measurement round. When resolving the inner degree of freedom, namely frequency ω, the photon-pair distribution exhibits interference fringes far beyond the coherence time [27,28], as described by [8,25],

$$P_\delta^\eta(\Delta t, \Delta\omega) = \frac{\mathcal{C}(\Delta\omega)}{2}\left(1 + \delta\eta^2 \cos(\Delta\omega\Delta t)\right), \tag{2}$$

where $\Delta\omega = \omega_1 - \omega_2$ is the difference in frequency and $\mathcal{C}(\Delta\omega)$ is the joint spectral distribution. For a fixed delay Δt, the output distributions in Eqs. (1) and (2) can be sampled by measuring both the bunching (N_B) and coincidence (N_C) outcomes. In addition, sampling the joint frequencies (ω_1, ω_2) is used to find the frequency difference $\Delta\omega$. The time delay Δt is then inferred through maximum likelihood estimation (MLE), see Supplemental Material [38] for more details.

The nonresolved estimation (NR) only requires the measurement of the total number of bunching (N_B) and coincidence (N_C) events [18,24]. The corresponding estimator can be expressed analytically,

$$\Delta t_{\mathrm{NR}}(N_C, N_B) = \frac{1}{\sigma}\sqrt{\log\left(\eta^2\frac{N_B + N_C}{N_B - N_C}\right)}. \tag{3}$$

In contrast, the frequency-resolved distribution given in Eq. (2) does not yield an analytic solution for Δt. Instead, we construct the estimator numerically via the likelihood function. Let the sample of N measured outcomes be denoted by $S_N = \{s^{\{i\}}\}_{i=1}^N$, where each $s^{\{i\}} = (\Delta\omega^{\{i\}}, \delta^{\{i\}})$ contains a frequency difference and the bunching or antibunching outcomes. The likelihood of a delay value Δt given the sample is defined as $\mathcal{L}_R(\Delta t|S_N) = P(S_N|\Delta t)$. The estimator $\widetilde{\Delta t}_{\mathrm{MLE}}$ is the value with the largest log-likelihood,

$$\mathcal{L}_R(\widetilde{\Delta t}_{\mathrm{MLE}}|S_N) = \sup_{\Delta t}\mathcal{L}_R(\Delta t|S_N). \tag{4}$$

The only unknown parameter remaining in Eq. (2) is η, which can be obtained during calibration. Therefore, the frequency-resolved scheme provides a numerical estimate of the time delay by matching the measured outcomes to the theoretical distribution via maximum likelihood. The error on these parameters will feed forward into the variance of the estimator, which we discuss in Supplemental Material [38]. A full derivation of the estimator in Eq. (4) is provided in Ref. [8].

Fisher information—We use Fisher information analysis to quantify the time-delay precision between the frequency-resolved and nonresolved methods. In the presence of both partial indistinguishability η and loss $(1 - \gamma)$, where $\gamma = 1$

for lossless detectors, the frequency-resolved Fisher information is [8],

$$\mathscr{F}_\eta = \mathbb{E}\left[\left(\frac{\mathrm{d}}{\mathrm{d}\Delta t}\log P^{\eta}_{\delta}(\Delta t,\Delta\omega)\right)^2\right] = \eta^4\gamma^2\int_{\mathbb{R}}\mathrm{d}\Delta\omega\,\mathcal{C}(\Delta\omega)^2\frac{\sin^2(\Delta\omega\Delta t)}{1-\eta^4\cos^2(\Delta\omega\Delta t)}. \quad (5)$$

The maximum information that can be attained over all possible measurement strategies is called the quantum Fisher information (QFI). For nonentangled photons with Gaussian spectra, the QFI is related to the spectral bandwidth by $\mathscr{H} = 2\sigma^2 = 1/2\tau^2$, which is half as much as for entangled photons [19,24].

To account for a finite frequency resolution, we model the Fisher information by dividing the frequency axis into discrete bins of width $2\delta\omega$, where $\delta\omega$ is the experimental spectral resolution, and we convolve the ideal joint spectrum with a triangular detector response function. Each bin n has a probability $P^{\eta}_{n,\delta}(\Delta t,\delta\omega,\sigma)$, and an associated Fisher information $\mathscr{F}_n(\Delta t)$, we then sum contributions from each bin to find the total Fisher information, see Supplemental Material [38] for more detail.

Reference [8] showed that, for Gaussian spectra and perfect indistinguishability, the frequency-resolved Fisher attains the quantum limit, $\mathscr{F}_{\eta=1}(\Delta t) = \mathscr{H}$. This demonstrates that when photons differ only in arrival time, the frequency-resolved scheme is optimal for extracting the most information from the photons. By contrast, the Fisher information for the nonresolved estimation method is given by [18,24],

$$\mathscr{F}^{\mathrm{NR}}_{\eta}(\Delta t) = \frac{\eta^4\gamma^2\mathscr{H}}{\exp\left(\frac{\Delta t^2}{2\tau^2}\right)-\eta^4}\frac{\Delta t^2}{2\tau^2}, \quad (6)$$

which rapidly decays for delays $\Delta t \gg \tau$, as the interference vanishes outside the coherence window. This is why $\mathscr{F}_\eta(\Delta t) \geq \mathscr{F}^{\mathrm{NR}}_{\eta}(\Delta t)$ holds, for $\eta < 1$, due to the convexity of the Fisher information and the marginalization over spectral modes [8].

Experimental methods—We perform the experiment using two configurations. The first uses a single photon pair source, which we refer to as twofold measurements when working in the coincidence regime. The second configuration uses two photon pair sources to herald independent photons, which we refer to as fourfold measurements. Each source consists of a domain-engineered, aperiodically poled KTP crystal [40,41], designed for group-velocity matching with a pulsed pump laser. This source generates spectrally pure, mutually indistinguishable photon pairs with Gaussian spectra centred on 1550 nm via spontaneous parametric down-conversion (SPDC) [42,43], see Supplemental Material [38]. We prepare the photons in identical quantum states by matching their frequency, polarization, and spatial mode, leaving only the relative time delay Δt at the beamsplitter to be varied using a mechanical translation stage with a reliable step size of 0.5 (μm).

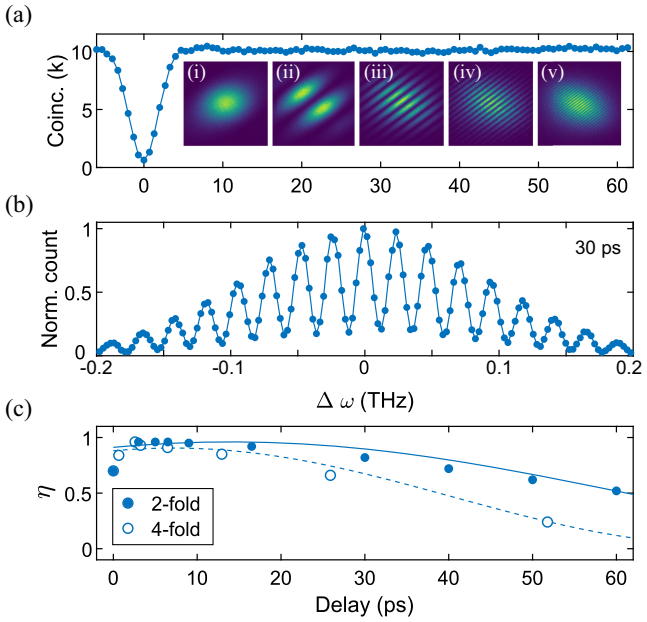


FIG. 2. Experimental calibration. (a) Two-photon coincidence counts (twofold) as a function of translation stage position over a 20 mm range, converted to delay (ps) and used to calibrate the prepared delays. Insets (i)–(v) show the joint spectral intensity (JSI) at delays 0,6,16,30,60 (ps). (b) Frequency marginal of inset (iv) with fringes fitted to Eq. (2) giving a visibility and indistinguishability of $\eta = 0.78$. (c) Indistinguishability η versus delay with data points used in the estimation protocol with a single source (solid) or independent sources (empty). Lines are plotted using a fitted spline.

Identifying *bunching* or *coincidence* outcomes is central to both estimation strategies. Pseudonumber resolving detectors are required to identify genuine bunching events. This is built from a fiber beam splitter and two superconducting nanowire detectors, see Supplemental Material [38] for more details.

To resolve the photon frequencies we use a time-of-flight spectrometer, comprising a 50 km fiber spool and a picosecond-resolution time-tagger, see Supplemental Material for details [38]. This setup achieves a spectral resolution $\delta\omega$ of $6.9/2\pi$ GHz, which sets the maximum bound on the delay range as $\Delta t \ll 144$ ps using the relation $\delta\omega \ll (1/|\Delta t|)$. The JSI for the bunching outcomes using a single source is plotted in Fig. 2(a). The marginal of the JSI reveals the interference visibility as a function of Δt. The visibility is related to the indistinguishability η through Eq. (2), which we find by fitting η to the distribution, see Fig. 2(c). We see that for larger delays, the photon indistinguishability goes down because a finer frequency resolution is required to erase all the distinguishable information between the photons. Furthermore, the

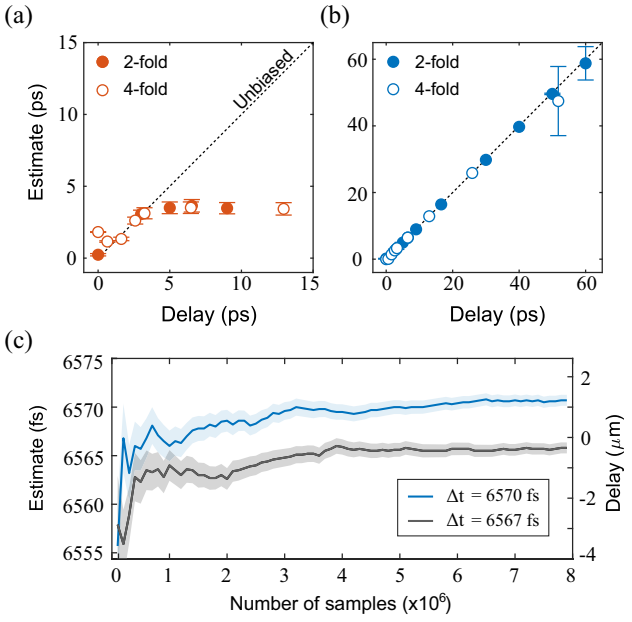


FIG. 3. Estimate accuracy and bias. (a) The nonresolved and (b) frequency-resolved (FR) estimates are plotted against the prepared delay to show the parameter dependence on the bias. Solid and hollow points indicate the single-source (twofold) and dual-source (fourfold) estimates. Error bars are calculated from one standard deviation of r rounds. (c) The cumulative FR-estimate of two delays shifted by three fs, each delay over five coherence lengths apart. The shaded area is the calculated standard deviation.

fourfold indistinguishability is lower due to additional noise from the extra detectors and a mismatch in parameters between the two sources.

Results—We evaluate the performance of the frequency-resolved and nonresolved estimates for both source configurations by comparing their accuracy and precision. Figure 3 shows the estimated delay plotted against the prepared delay for both methods using 450 mW pump power. Each data point represents the average over r repeat estimates, each using N samples. The twofold estimates use $r = 1000$ repeats and $N = 1000$ samples, while the fourfold estimates use $r = 100$ repeats and $N = 100$ samples. As expected, the nonresolved estimates are only unbiased up to 3 ps, before the estimates begin to fail. In comparison, the averaged frequency-resolved estimate is relatively unbiased up to 60 ps, but its variance increases as shown by the large error bars.

The frequency-resolved method is capable of precision sensing well outside the photon coherence time, where the nonresolved method fails. We measure a three-femtosecond shift between two temporal delays at around five times the coherence time, see Fig. 3(c). We pick a reference delay at 6.567 ps and translate the delay stage by one micron, or 3 fs. We use 100 mW pump power and 7.9 million samples to estimate the delay at each position with an uncertainty of 0.5 fs (≈168 nm). We measured a shift of 4 fs, with an error of 1 fs. The discrepancy is most likely from the reliability of the delay stage.

We evaluate the precision using the experimental metrological information $\mathcal{I}$, defined via the Cramér-Rao bound [44,45]

$$\mathrm{Var}(\widetilde{\Delta t}) \geq \frac{1}{N\mathcal{I}}, \tag{7}$$

where N is the number of trials in which *both* photons are detected and $\mathcal{I}$ is the Fisher information per successful two-photon event. Our estimators rely on two-photon interference (bunching and coincidences at the beam splitter), so events in which one photon is lost do not contribute information within this scheme and are discarded. We discuss this further in the discussion and Supplemental Material [38]. To benchmark the experiment against the theoretical limit under the same conditions, we will use the conditional quantum Fisher information [24] $\mathscr{H}_c = \gamma^2\mathscr{H}$, where γ^2 is the probability that both photons are detected and $\mathscr{H}$ is the ideal two-photon QFI. The ratio of the experimentally obtained information to the conditional QFI is plotted in Fig. 4(a). The maximum obtainable information for all strategies occurs around short delays, approximately 1 ps, and decays exponentially with increasing delay in the non-frequency-resolved case, while it decays polynomially in the frequency-resolved estimates. The experimentally obtained data points agree well with the theoretical model, see caption for details, although the fourfold estimates yield lower metrological information than the twofold data, primarily because of reduced photon indistinguishability and also additional noise arises from the dual-source setup with additional fibers.

Photon indistinguishability plays a critical role in both estimation strategies, as $\mathscr{F} \propto \eta^4$. Our probabilistic SPDC sources generate higher-order photon emission with probability p^2, where $p \approx 0.0112$ is the photon-pair emission probability per pulse. This adds decoherence and decreases the two-photon interference visibility. This can be controlled by the squeezing parameter of our sources, mostly by the pump power and focussing condition. To maximize $\mathcal{I}$, we reduced the pump power to 100 mW, thereby decreasing the multiphoton contribution and increasing the indistinguishability. At this pump power we measure $\eta = 0.981 \pm 0.005$, and the experimentally obtained metrological information reaches $\mathcal{I} = 0.442$ (ps^{-2}),blue triangles in Fig. 4(c), which corresponds to 85% the conditional QFI.

Despite the frequency-resolved metrological information decaying with larger delays, the relative performance is still maintained because the estimator is not biased. To demonstrate this, we calculate the mean squared error (MSE), via $\mathrm{MSE}(\widetilde{\Delta t}) = \mathbb{E}[(\widetilde{\Delta t} - \Delta t)^2]$. This includes both the estimator bias and variance. The ratio of nonresolved to frequency-resolved MSE is plotted in Fig. 4(b) and exceeds

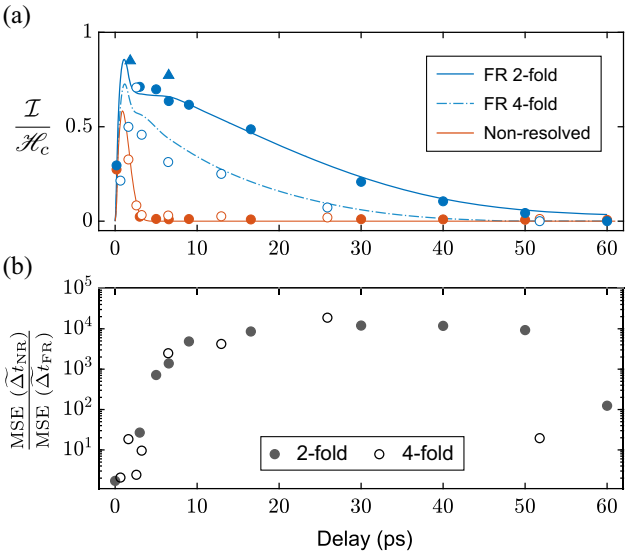


FIG. 4. Metrological information. (a) Ratio of experimental Fisher information to conditional QFI for the FR and nonresolved estimators. Filled symbols are twofold data, while empty symbols are fourfold data, and triangles twofold FR data at 100 mW. The orange curve is the nonresolved Fisher information from Eq. (6) with $\eta = 0.97$, and the blue curve is the frequency-resolved Fisher information from Eq. (5) with $\eta(\Delta t)$ taken from the fit in Fig. 2(c) (see Supplemental Material [38]). (b) Sensing advantage is quantified by the ratio of the FR and nonresolved mean squared errors.

four orders of magnitude for estimates between 16 and 50 ps.

Discussion—Conventional HOM sensing typically requires two full delay scans; one to record a reference interference fringe as in Fig. 2(a), and a second scan with the sample inserted to measure the induced shift. In such scans, most detected photons provide little information about the sample-induced delay. The two methods analyzed here are scan-free and extract information from the detected photons more efficiently, requiring only an initial calibration. This is advantageous for capturing fast dynamics, which may be lost during scanning. In the nonresolved method, the dynamic range is limited by the photon coherence time. By contrast, in the frequency-resolved method, the limiting factor is the detector's frequency resolution, which removes the constraint imposed by the temporal width. This enables operation over a large dynamic range, which opens a route to microscopy and sensing at larger scales.

The achievable precision depends on both the spectral bandwidth and the resolution of the frequency-resolved detectors, which can be improved in future experiments. We estimate that improving the spectral resolution by a factor of ten will extend the dynamic range by a further factor of ten. The precision can also be enhanced using entangled photon pairs to realize a $\sqrt{2}$ improvement per sample [46]. Further gains are possible with spectrally engineered sources that use detuned biphoton schemes [19,20], which can provide large Fisher information without fringe tracking or calibration, overcoming the sensitivity trade-off in optical sensors [47,48]. Surprisingly, photons with a larger spectral bandwidth provide a higher Fisher information without a penalty on the dynamic range, unlike the nonresolved method.

A limitation of our present setup is fiber loss from our time-of-flight spectrometer, which is approximately 99% for two 50 km fiber spools. One might expect that a direct time of flight estimate without such high loss would outperform the frequency-resolved method, but we show in Supplemental Material [38] that this is not the case. Also, if the dispersive fiber is placed before the optical delay line, this loss occurs before the probes are encoded by the sample. In the resource counting of Giovannetti *et al.* [49], this reduces the number of prepared probes but not the Fisher information per encoded probe. Alternatively, commercial single-photon spectrometers with lower loss could be employed. The frequency-resolved protocol itself is agnostic to the physical platform and could equally be implemented with a chirped fiber Bragg grating [26] or a diffraction grating combined with a photodiode array [37,46], although the spectral resolution of these devices is typically lower than that achievable with long dispersive fibers.

Another advantage of our technique is the robustness to phase noise and imbalanced losses [23], a characteristic of two-photon interference, which is sensitive to the wave packet group delay, rather than the phase delay. This method achieves a measurement precision comparable to phase-based methods but without active stabilization [2,13] or the phase wrapping problem, which requires additional phase tracking algorithms [50,51].

The analysis of this report has relied on assumptions about the photon sources and detection efficiency. SPDC sources are intrinsically probabilistic, and post selection is therefore always used to identify genuine photon pairs when measuring two-photon interference. Although standard in quantum metrology [52–58], this approach imposes a metrological penalty because the precision is evaluated only on trials with successful detections, which does not fully account for losses. A more complete metric is the number of probes encoded by the sample [49], which naturally incorporates penalties from imperfect heralding, optical loss, and detector inefficiency. However, in this Letter, both estimation methods rely on postselection in the same way, so the comparative conclusions remain unaffected. This Letter could be improved with a full loss-inclusive analysis as demonstrated in recent works [59,60], but requires high heralding efficiencies above 70% and low-loss, high-efficiency detectors to gain an unconditional quantum enhancement.

Conclusion—We have demonstrated a frequency-resolved two-photon interference protocol for optical delay sensing

that achieves nanometer scale precision with a dynamic range more than an order of magnitude larger than conventional nonresolved Hong-Ou-Mandel schemes. By analyzing the Fisher information for the frequency-resolved estimation, we show that this implementation operates near the quantum limit for the relevant loss model, without adaptive measurements or active phase stabilization. This implementation is scan-free and robust to phase noise or imbalanced losses, offering a practical route to nanoscale optical sensing.

Acknowledgments—We thank A. Pickston for helpful discussions and the referees' comments for improving this manuscript. This work was supported by the UK Engineering and Physical Sciences Research Council (Grant No. EP/T001011/1.). L. M. acknowledges partial support by Xairos Systems Inc. V. T. acknowledges partial support from the Air Force office of Scientific Research under Award No. FA8655-23-1- 7046.

R. M. J. B., A. F., and V. T. conceived the project. R. M. J. B., T. J., and J. H. performed the experiment, R. M. J. B., T. J., and L. M. analyzed the results. L. M. and V. T. developed the theoretical tools used in the analysis. All authors contributed to writing and revisions of the manuscript.

The authors declare no competing financial or nonfinancial interests.

Data availability—The data are not publicly available. The data are available from the authors upon reasonable request.

[1] C.-K. Hong, Z.-Y. Ou, and L. Mandel, Phys. Rev. Lett. **59**, 2044 (1987).
[2] J. Rarity and P. Tapster, in *Photons and Quantum Fluctuations* (CRC Press, Boca Raton, Florida, 2020), pp. 122–150.
[3] V. Tamma and S. Laibacher, Phys. Rev. Lett. **114**, 243601 (2015).
[4] J.-W. Pan, D. Bouwmeester, H. Weinfurter, and A. Zeilinger, Phys. Rev. Lett. **80**, 3891 (1998).
[5] E. Knill, R. Laflamme, and G. J. Milburn, Nature (London) **409**, 46 (2001).
[6] D. E. Browne and T. Rudolph, Phys. Rev. Lett. **95**, 010501 (2005).
[7] S. Pirandola, B. R. Bardhan, T. Gehring, C. Weedbrook, and S. Lloyd, Nat. Photonics **12**, 724 (2018).
[8] D. Triggiani, G. Psaroudis, and V. Tamma, Phys. Rev. Appl. **19**, 044068 (2023).
[9] S. Laibacher and V. Tamma, Phys. Rev. Lett. **115**, 243605 (2015).
[10] S. Muratore, D. Triggiani, and V. Tamma, Phys. Rev. Appl. **23**, 054033 (2025).
[11] J. Ho, J. W. Webb, R. M. Brooks, F. Grasselli, E. Gauger, and A. Fedrizzi, arXiv:2410.00970.
[12] T. Faleo, E. Brunner, J. W. Webb, A. Pickston, J. Ho, G. Weihs, A. Buchleitner, C. Dittel, G. Dufour, A. Fedrizzi *et al.*, Sci. Adv. **10**, eadp9030 (2024).
[13] H. Fearn and R. Loudon, J. Opt. Soc. Am. B **6**, 917 (1989).
[14] A. M. Steinberg, P. G. Kwiat, and R. Y. Chiao, Phys. Rev. Lett. **71**, 708 (1993).
[15] D. Branning, A. L. Migdall, and A. V. Sergienko, Phys. Rev. A **62**, 063808 (2000).
[16] E. Dauler, G. Jaeger, A. Muller, A. Migdall, and A. Sergienko, J. Res. Natl. Inst. Stand. Technol. **104**, 1 (1999).
[17] A. M. Steinberg, P. G. Kwiat, and R. Y. Chiao, Phys. Rev. A **45**, 6659 (1992).
[18] A. Lyons, G. C. Knee, E. Bolduc, T. Roger, J. Leach, E. M. Gauger, and D. Faccio, Sci. Adv. **4**, eaap9416 (2018).
[19] Y. Chen, M. Fink, F. Steinlechner, J. P. Torres, and R. Ursin, npj Quantum Inf. **5**, 43 (2019).
[20] C. P. Lualdi, S. J. Johnson, M. Vayninger, K. A. Meier, S. Sahoo, S. I. Bogdanov, and P. G. Kwiat, Sci. Adv. **11**, eadw4938 (2025).
[21] S. Pellegrini, G. S. Buller, J. M. Smith, A. M. Wallace, and S. Cova, Meas. Sci. Technol. **11**, 712 (2000).
[22] J. Rapp, Y. Ma, R. M. Dawson, and V. K. Goyal, Optica **8**, 30 (2021).
[23] H. Scott, D. Branford, N. Westerberg, J. Leach, and E. M. Gauger, Phys. Rev. A **104**, 053704 (2021).
[24] H. Scott, D. Branford, N. Westerberg, J. Leach, and E. M. Gauger, Phys. Rev. A **102**, 033714 (2020).
[25] S. Laibacher and V. Tamma, Phys. Rev. A **98**, 053829 (2018).
[26] V. V. Orre, E. A. Goldschmidt, A. Deshpande, A. V. Gorshkov, V. Tamma, M. Hafezi, and S. Mittal, Phys. Rev. Lett. **123**, 123603 (2019).
[27] T. Gerrits, F. Marsili, V. B. Verma, L. K. Shalm, M. Shaw, R. P. Mirin, and S. W. Nam, Phys. Rev. A **91**, 013830 (2015).
[28] R.-B. Jin, T. Gerrits, M. Fujiwara, R. Wakabayashi, T. Yamashita, S. Miki, H. Terai, R. Shimizu, M. Takeoka, and M. Sasaki, Opt. Express **23**, 28836 (2015).
[29] R.-B. Jin, R. Shimizu, T. Ono, M. Fujiwara, G.-W. Deng, Q. Zhou, M. Sasaki, and M. Takeoka, arXiv:2104.01062.
[30] L. Maggio, D. Triggiani, P. Facchi, and V. Tamma, Eur. Phys. J. Plus **140**, 954 (2025).
[31] D. Triggiani and V. Tamma, Phys. Rev. A **111**, 032605 (2025).
[32] D. Triggiani and V. Tamma, Phys. Rev. Lett. **132**, 180802 (2024).
[33] L. Maggio, D. Triggiani, P. Facchi, and V. Tamma, Phys. Scr. **100**, 035106 (2025).
[34] M. O. Scully and K. Drühl, Phys. Rev. A **25**, 2208 (1982).
[35] Y.-H. Kim, R. Yu, S. P. Kulik, Y. Shih, and M. O. Scully, Phys. Rev. Lett. **84**, 1 (2000).
[36] Y. Chen, Q. Shen, S. Luo, L. Zhang, Z. Chen, and L. Chen, Phys. Rev. Appl. **17**, 014010 (2022).
[37] F. Di Lena, F. Sgobba, D. Triggiani, A. Andrisani, C. Lupo, P. Daniele, G. Fratta, G. Acconcia, I. Rech, and L. S. Amato, arXiv:2506.03098.
[38] See Supplemental Material at http://link.aps.org/supplemental/10.1103/6xy6-c2yd for a detailed experimental setup, loss model, and theoretical derivations.
[39] A. M. Brańczyk, arXiv:1711.00080.

[40] A. Pickston, F. Graffitti, P. Barrow, C. L. Morrison, J. Ho, A. M. Brańczyk, and A. Fedrizzi, Opt. Express **29**, 6991 (2021).
[41] F. Graffitti, P. Barrow, M. Proietti, D. Kundys, and A. Fedrizzi, Optica **5**, 514 (2018).
[42] F. Graffitti, J. Kelly-Massicotte, A. Fedrizzi, and A. M. Brańczyk, Phys. Rev. A **98**, 053811 (2018).
[43] F. Graffitti, D. Kundys, D. T. Reid, A. M. Brańczyk, and A. Fedrizzi, Quantum Sci. Technol. **2**, 035001 (2017).
[44] W. Feller, Ann. Math. Stat. **18**, 136 (1947).
[45] V. K. Rohatgi and A. M. E. Saleh, *An Introduction to Probability and Statistics* (John Wiley & Sons, New York, 2015).
[46] C. Chen, Y. Chen, and L. Chen, Phys. Rev. Appl. **19**, 054092 (2023).
[47] N. Bobroff, Meas. Sci. Technol. **4**, 907 (1993).
[48] J. Fraden, *Handbook of Modern Sensors: Physics, Designs, and Applications* (Springer, New York, 2004).
[49] V. Giovannetti, S. Lloyd, and L. Maccone, Nat. Photonics **5**, 222 (2011).
[50] K. Itoh, Appl. Opt. **21**, 2470 (1982).
[51] M. Hayashi, S. Vinjanampathy, and L. C. Kwek, J. Phys. B **52**, 015503 (2018).
[52] P. Walther, J.-W. Pan, M. Aspelmeyer, R. Ursin, S. Gasparoni, and A. Zeilinger, Nature (London) **429**, 158 (2004).
[53] M. W. Mitchell, J. S. Lundeen, and A. M. Steinberg, Nature (London) **429**, 161 (2004).
[54] T. Nagata, R. Okamoto, J. L. O'brien, K. Sasaki, and S. Takeuchi, Science **316**, 726 (2007).
[55] B. L. Higgins, D. W. Berry, S. D. Bartlett, H. M. Wiseman, and G. J. Pryde, Nature (London) **450**, 393 (2007).
[56] K. J. Resch, K. L. Pregnell, R. Prevedel, A. Gilchrist, G. J. Pryde, J. L. O'Brien, and A. G. White, Phys. Rev. Lett. **98**, 223601 (2007).
[57] W.-B. Gao, C.-Y. Lu, X.-C. Yao, P. Xu, O. Gühne, A. Goebel, Y.-A. Chen, C.-Z. Peng, Z.-B. Chen, and J.-W. Pan, Nat. Phys. **6**, 331 (2010).
[58] L.-Z. Liu, Y.-Z. Zhang, Z.-D. Li, R. Zhang, X.-F. Yin, Y.-Y. Fei, L. Li, N.-L. Liu, F. Xu, Y.-A. Chen *et al.*, Nat. Photonics **15**, 137 (2021).
[59] S. Slussarenko, M. M. Weston, H. M. Chrzanowski, L. K. Shalm, V. B. Verma, S. W. Nam, and G. J. Pryde, Nat. Photonics **11**, 700 (2017).
[60] S.-R. Zhao, Y.-Z. Zhang, W.-Z. Liu, J.-Y. Guan, W. Zhang, C.-L. Li, B. Bai, M.-H. Li, Y. Liu, L. You *et al.*, Phys. Rev. X **11**, 031009 (2021).